



# The Advanced Scintillator Compton Telescope (ASCOT)

P. Bloser<sup>1</sup>, T. Sharma<sup>2</sup>, J. Legere<sup>2</sup>, C. Bancroft<sup>2</sup>, C. Frost<sup>2</sup>, M. McConnell<sup>2,3</sup>,  
J. Ryan<sup>2</sup>, and A. Wright<sup>2</sup>

<sup>1</sup> Los Alamos National Laboratory, P.O. Box 1663, Los Alamos, NM 87545, USA  
e-mail: [pbloser@lanl.gov](mailto:pbloser@lanl.gov)

<sup>2</sup> University of New Hampshire, Space Science Center, 8 College Road, Durham, NH 03824, USA

<sup>3</sup> Southwest Research Institute, Department of Earth, Oceans, and Space, 8 College Road, Durham, NH 03824, USA

**Abstract.** There is a need in high-energy astronomy for new soft- to medium-energy gamma-ray observations, ideally covering the energy range from 0.3 – 100 MeV, to expand on the success of the COMPTEL instrument on CGRO. As this is a particularly difficult energy range to study, progress has been slow in the medium-energy band, despite the important contributions of INTEGRAL in gamma-ray lines and polarimetry. Gamma-ray astronomy communities around the world are actively studying a multitude of technological approaches to close the MeV “Sensitivity Gap”. One such approach is to build directly on the legacy of COMPTEL by using modern, fast scintillators that improve instrument response while preserving time-of-flight background rejection. Fortunately, high-performance scintillators, such as Cerium Bromide and p-terphenyl, and compact light readout devices, such as silicon photomultipliers (SiPMs), are commercially available and capable of meeting this need. The University of New Hampshire has constructed an Advanced Scintillator Compton Telescope (ASCOT) with SiPM readout, with the goal of demonstrating this technology by imaging the Crab Nebula at MeV energies during a high-altitude balloon flight. The ASCOT balloon payload was launched from Palestine, TX, on July 5, 2018, and operated successfully at a float altitude of ~ 122,000 feet for five hours while the Crab was high in the sky. We present the motivation for the ASCOT concept, describe the instrument and balloon payload, and provide a preliminary overview of the flight data.

**Key words.** Gamma rays: general – Instrumentation: detectors – Methods: observational – Balloons – Telescopes

## 1. Introduction

The field of gamma-ray astronomy in the medium-energy band (~ 0.3 – 100 MeV) has been stagnant since the demise of COMPTEL in 2000 (Schönfelder et al. 1993). While

INTEGRAL has achieved many notable successes in gamma-ray lines, and has helped to pioneer gamma-ray polarimetry, it has not significantly improved on the continuum sensitivity of COMPTEL above 1 MeV. The need for new, more sensitive observations is widely

recognized, and a variety of technological approaches are being pursued around the world (Rando et al. 2017; de Angelis et al. 2018).

Compton telescopes remain the instrument of choice for performing imaging and spectroscopy in this difficult energy range, owing to the fact that the coincidence requirement and inherent directionality serve to suppress the intense backgrounds generated by cosmic ray interactions in any space-borne instrument. COMPTEL employed two detector arrays separated by 1.6 m. Compton scatters in the forward detector (D1) were measured for location, energy deposit, and pulse shape. D1 was composed of liquid organic scintillator and read out by photo-multiplier tubes (PMTs). Location and energy deposit were similarly measured for scatters into the rearward detector (D2), and the time-of-flight (ToF) was measured. D2 was composed of dense, inorganic NaI(Tl) scintillator. From the positions and energy deposits in the two detectors, the source of the incident gamma-ray photon could be constrained to lie on an “event circle” on the sky using the Compton scattering formula. Only events with a ToF value corresponding to a forward-scattered photon were selected; this proved crucial to achieving a useful signal-to-noise ratio.

We are pursuing a technological approach to MeV astronomy that builds directly on the legacy of COMPTEL: using modern, fast scintillator materials coupled to silicon photomultipliers (SiPMs) to construct a more capable Compton telescope that retains ToF background rejection. The most recent product of this effort is the Advanced Scintillator Compton Telescope (ASCOT) balloon payload (Sharma et al. 2017; Bloser et al. 2018). Here we describe the ASCOT instrument and present initial results from the successful balloon flight that took place on 5 July 2018 with the goal of imaging the Crab Nebula at MeV energies.

## 2. The ASCOT instrument

The ASCOT instrument is illustrated via an exploded engineering drawing in Fig. 1. The telescope is composed of detector “modules”, each

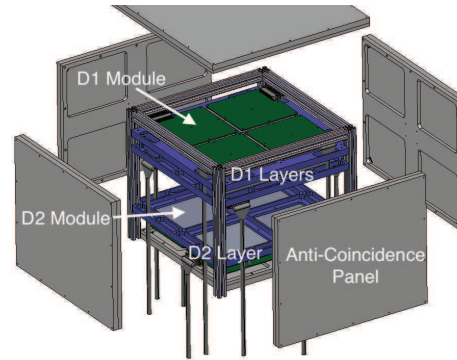


**Fig. 1.** Exploded view of the ASCOT instrument.

containing an  $8 \times 8$  array of scintillator elements. Each scintillator element is  $15 \times 15 \times 25$  mm<sup>3</sup> and is read out by a  $2 \times 2$  array of 6-mm commercial SiPMs. A  $2 \times 2$  array of modules forms an instrument layer. There are two D1 layers and (for reasons of cost) one D2 layer. The separation between the lower D1 layer and the D2 layer is  $\sim 13$  mm center-to-center; simulations indicate that this separation provides the best sensitivity to the Crab Nebula from balloon altitudes for an instrument of this size by enhancing efficiency at the expense of optimal ToF discrimination (Bloser et al. 2018).

The D1 module (Fig. 2) scintillators are made of p-terphenyl, an organic crystal with high light output, fast decay time, and good pulse-shape discrimination capability for distinguishing gamma-ray and neutron interactions (Matei et al. 2012). The p-terphenyl was purchased from Proteus, Inc., and assembled into arrays inside plastic (Delrin) housings that are not susceptible to activation. The scintillators are separated by slats of white Gigahertz Optik material.

The D2 module (Fig. 3) elements are made of CeBr<sub>3</sub>, an inorganic scintillator with good stopping power, fast decay time, and excellent energy resolution (Shah et al. 2005). The D2 modules were purchased from Berkeley Nucleonics Corporation/Scionix, who sealed the hygroscopic material inside hermetic, vacuum-rated aluminum housing with a com-

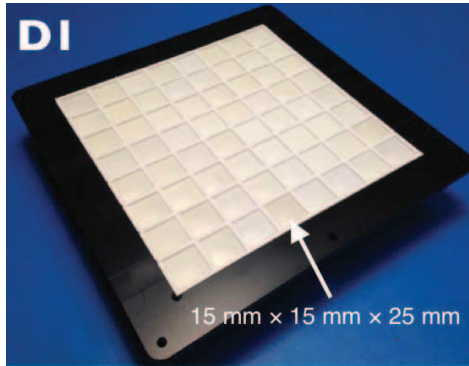


**Fig. 2.** D1 module composed of organic p-terphenyl elements.

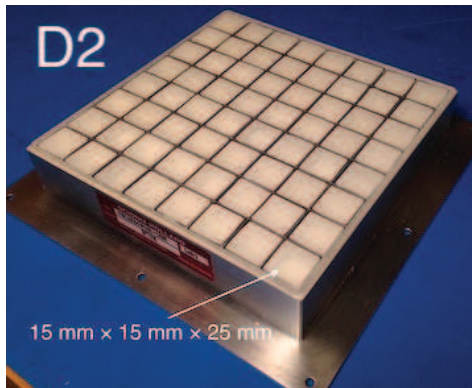


**Fig. 3.** D2 module composed of  $\text{CeBr}_3$  elements in a hermetic package with a common optical window.

mon optical window. This common window resulted in some light loss and optical cross talk.

The scintillators are read out by summed,  $2 \times 2$  arrays of MicroFC-60035-SMT SiPMs purchased from SensL Corp. The SiPMs were mounted on custom “strip boards,” each of which reads out one row of a detector module. The strips were plugged into module array boards (Fig. 4) that provided front-end electronics and bias voltage ( $\sim 29$  V) with temperature-based gain correction. The array boards were designed to be mechanically mounted to the module housings, and the SiPMs were optically coupled to the scintillators (or optical window) using Eljen EJ-560 silicone rubber optical pads.



**Fig. 4.** Module array board partially populated with four rows of SiPM strip boards.

After integration, calibration measurements were performed using radioactive sources to measure the instrument’s performance. The D1 detectors achieve a trigger threshold of  $\sim 35 - 40$  keV and an energy resolution of  $\sim 30\%$  (FWHM) at 60 keV. The D2 detectors show a typical energy resolution of  $\sim 6\%$  (FWHM) at 662 keV, and the trigger threshold was set to 200 keV. Between single pixel pairs the ToF resolution is dependent on the two energy deposits; the best value recorded is  $\sim 480$  ps (FWHM) for events with  $\sim 300$  keV in D1 and  $\sim 1400$  keV in D2. Cross-talk effects begin to degrade the D1 timing resolution for energies  $> 500$  keV.

To suppress charged particle background, the detector layers are surrounded on six sides by anti-coincidence panels (Fig. 1) made of plastic scintillator with SiPM readouts in the corners. The panels are housed in plastic Delrin frames to avoid activation. In addition, a tagged calibration source is mounted at the center of the D2 layer to provide in-flight monitoring of the detector gains. The tagged source consists of a plastic scintillator button infused with  $^{60}\text{Co}$  and read out by a SensL SiPM.

### 3. The ASCOT balloon payload

The ASCOT balloon payload is shown in Fig. 5 after integration in the field. The instru-

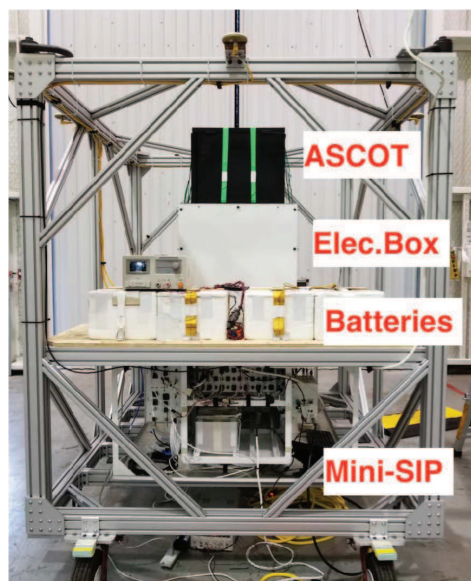


**Fig. 5.** ASCOT balloon payload assembled in the field.

ment is mounted, zenith-pointed, on top of the electronics box in a simple gondola made of extruded aluminum T-slot elements. Batteries and other electronics are mounted to the sides and below. No attitude control was required; attitude knowledge was provided by an ADU5 GPS compass.

During payload integration radioactive sources were suspended by a crane at various positions above the instrument to provide a full-telescope imaging test. The gamma-ray image in the far field (i.e., produced by back-projection of the Compton event circles onto an infinite sphere in angular coordinates) of a  $^{252}\text{Cf}$  source is shown in Fig. 6; the source position (black cross) is correctly reproduced.

#### 4. Balloon flight

The ASCOT payload was launched by NASA's Columbia Scientific Balloon Facility from Palestine, TX on 5 July 2018 (Fig. 7). The payload achieved a float altitude between 119,000 and 123,000 feet (36.3 – 37.5 km) and maintained it for 5 hours (Fig. 8). During this time

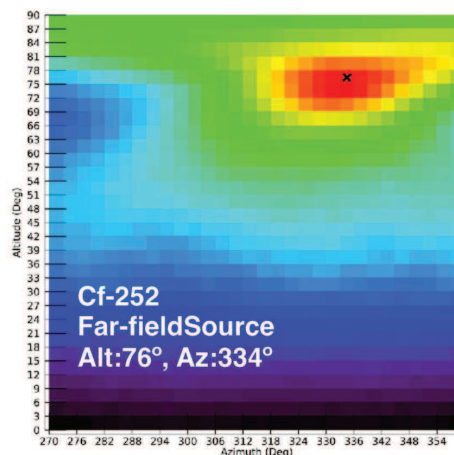


**Fig. 6.** The ASCOT gamma-ray image of a  $^{252}\text{Cf}$  source correctly reconstructs the source location (black cross).

the Crab Nebula was high in the sky. All components of the payload operated successfully during the flight, and data from the tagged calibration source indicates that the instrument gain remained stable (within  $\sim 2\%$ ) throughout (Fig. 9). Following termination, the payload was successfully recovered in West Texas and transported back to the University of New Hampshire, where initial checkouts indicated that all detector modules are still in working order.

The detailed analysis of the flight data is underway. The analysis steps will include the correction of pre-flight energy calibrations using the tagged source data; the analysis and application of pulse-shape discrimination cuts for D1 events to reject atmospheric neutron interactions; and the complete analysis of ToF calibration data and the optimization of ToF cuts to maximize sensitivity to the Crab in the flight data. We will then perform detailed Monte Carlo simulations of the instrument response in order to produce maps of the gamma-ray sky in the vicinity of the Crab Nebula, using maximum likelihood and other imaging techniques commonly applied to Compton telescope data (Lowell et al. 2017).



**Fig. 7.** ASCOT was successfully flown in July of 2018 from Palestine, TX.

## 5. Conclusions

The ASCOT balloon flight has successfully demonstrated operation of advanced scintillator/SiPM detector technology, configured as a Compton telescope, in a near-space environment. The complete analysis of the calibration and flight data is underway, and we expect to detect the Crab Nebula from 0.2 – 2 MeV at a significance of  $\sim 4\sigma$ .

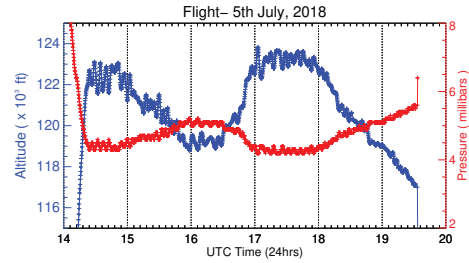


**Fig. 8.** ASCOT remained at float for  $\sim 5$  hours while the Crab Nebula was high in the sky.

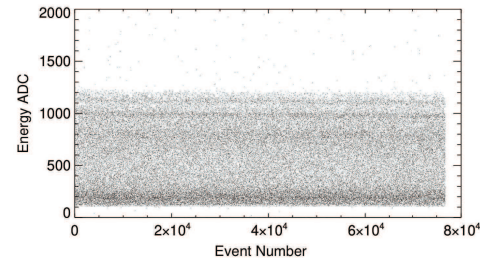


**Fig. 9.** Tagged source events in D2 indicate that the instrument gain remained stable.

*Acknowledgements.* This work was supported by NASA Grant NNX15AE49G. We heartily thank the staff of NASA's Columbia Scientific Balloon Facility for the successful balloon campaign.

## References

- Bloser, P., et al. 2018, Proc. SPIE, 10699, 106995X
- de Angelis, A., et al. 2018, JHEAp, 19, 1
- Loewll, A., et al. 2017, ApJ, 848, 119
- Matei, C., et al. 2012, NIM-A, 676, 135
- Rando, R. 2017, JINST, 12, C11024
- Schönfelder, V., et al. 1993, ApJS, 86, 657
- Shah, K., et al. 2005, IEEE Trans. Nucl. Sci., 52, 3157
- Sharma, T., et al. 2017, Proc. SPIE, 10397, 103970L